Palaeozoic orogeneses around the Siberian craton: Structure and evolution of the Patom belt and foredeep

Thomas de Boisgrollier, Carole Petit, Marc Fournier, P. Leturmy, Jean-Claude Ringenbach, Vladimir A. San'Kov, Svetlana A. Anasimova, Sergei N. Kovalenko

Palaeozoic orogeneses around the Siberian craton : structure and evolution of the Patom belt and foredeep

T. de Boisgrollier[1], C. Petit[1], M. Fournier[1], P. Leturmy[2], J.-C. Ringenbach[3], V.A. San'kov[4], S.A. Anisimova[4] and S.N. Kovalenko[4]

[1] *Laboratoire de Tectonique - CNRS UMR 7072, Université Pierre et Marie Curie - Paris 6, case 129, 4 place Jussieu, 75252 Paris Cedex 05, France*

[2] *Laboratoire de Tectonique - CNRS UMR 7072, Université de Cergy-Pontoise, Bâtiment Neuville III.1, 5 mail Gay Lussac, Neuville-sur-Oise, 95031 Cergy-Pontoise Cedex, France*

[3] *Total TG/ISS/STRU, CSTJF, avenue Larribau, 64000 Pau, France*

[4]*Institute of the Earth Crust, Russian Academy of Science, Siberian Branch, 128 Lermontova street, 664033 Irkutsk, Russia*

ABSTRACT

This paper sheds light on the evolution of the Patom belt. This mountain range draws an arc along the south-eastern edge of the Siberian craton. It is supposed to be of Caledonian age and to result from the accretion of microcontinents against the craton, but up to now, its detailed stratigraphic and tectonic history was unclear. A field study allows us to precise it. The sedimentary record is marked by a slow evolution with stable periods of more than 250 Ma. The observed sedimentary succession confirms the existence of a passive margin setting in the Late Riphean (900 Ma), followed during the Vendian (650-600 Ma) by the obduction of the Baikal-Muya ophiolites belt and a foredeep inversion. After then, a late Cambrian extension occurred, which is first described in this paper. The second collision stage occurred after 385 Ma, in the late Devonian-Early Carboniferous. Sedimentary and tectonic data are interpreted in the light of the geodynamic evolution of Siberia, which is dominated by continental collages against the Siberian craton. Field data reveal a homogeneous direction of

compression from the inner areas to the foreland. Whereas the inner range displays metamorphosed units deformed in the ductile domain, deformation is weaker in the foreland, which developed above the cratonic crust. We relate this high deformation gradient to the presence of the stiff craton which impeded strain propagation. The irregular shape of the craton as well as pre-existent basement topography can explain the different tectonic styles observed along the belt.

1. INTRODUCTION

Pericratonic mountain ranges result from the accretion against Archaean cratons of exotic blocs or "terranes" of various origins. This is one of the processes responsible for continental growth. These cratonic collages are evidenced in many mountain ranges, as in North American Cordilleras (*Coney et al., 1980; Monger, 1997; English and Johnston, 2005; Johnston and Borel, 2007*) or SE Asian Pacific belt (*Pubellier, 2003*), by the imbrication of various units consisting of continental fragments, island arcs remnants, marginal basins, oceanic plateaus, ophiolitic belts or volcanic mélanges, depending on their various pre-collisional histories.

Pericratonic orogens are specific for following reasons: first, the pericratonic setting is associated with the presence of a cold and strong lithosphere on the cratonic side of the orogen. The associated deformation is consequently very localized and short-lived because it can not propagate within the cratonic lithosphere which behaves rigidly (e.g., *Burov and Diament, 1995*). Second, repeated continental accretions imply successive jumps of the deforming zone towards the newly formed continent boundary. Such an evolution does not allow the formation of mature mountain ranges.

The Patom range is located at south-eastern edge of the Siberian craton (Fig. 1A). It draws an arc of almost 1000 kilometers long, from the northern end of the Baikal Lake in the South-West to the Stanovoy range in the North-East. Lake Baikal is a part of the Cenozoic Baikal Rift System, whose northern part crosses the Patom range in a succession of rhombohedral basins between the lake and the Stanovoy range. The morphology of the Patom range is well preserved in the topography, with a 1000 to 1500 m-high inner domain defining the so-called “Patom highland” separated from the flat Siberian craton (~500 m) by a topographic step corresponding to the main frontal thrust.

This fold and thrust belt is a segment of the Central Asian Orogenic Belt (Fig. 1A) and was formed during the evolution and closure of the Palaeo-Asian ocean, in the Late Proterozoic-Palaeozoic time (*Sengör et al., 1993; Buchan et al., 2002; Dobretsov et al., 2003; Kröner et al., 2005; Belichenko et al. 2006; Gordienko, 2006; Windley et al., 2007*). It is generally admitted that the Central Asian Orogenic Belt results from a long history of arc and microcontinent accretion, even if the evolutionary models are still discussed (*Khain et al., 2003; Kröner et al., 2005; Helo et al., 2006*). In particular, many questions remain concerning the nature and contours of the terranes involved, the timing of deformations, and the geodynamics of the Patom range (*Belichenko et al., 2006*). The sinuous geometry of this fold and thrust belt seems to be influenced by a pre-existing curved shape of the Siberian craton's margin (commonly referred to as the "Vitim embayment"), but the exact role of inherited structures is not well known. In this paper, we bring new constraints on structure and evolution of Patom fold and thrust belt from stratigraphic and tectonic data acquired during three field seasons in 2005, 2006 and 2007. A synthetised stratigraphy from Riphean (Neoproterozoic) to Jurassic is used to determine regional correlations and identification of major tectonical or geodynamical events. We then present results of a multi-scale structural analysis, both considering the foreland basin and the inner range geometry and deformation. Finally, we propose a geodynamic interpretation of these observations in the context of a pericratonic mountain range.

2. MAIN UNITS OF THE PATOM FOLD AND THRUST BELT

The Patom fold and thrust belt is classically divided into two main domains (Fig. 2). The foreland (outer) domain is made up of the Siberian craton and its margin, where the Neoproterozoic-Palaeozoic sedimentary cover is folded with large Ordovician-Devonian cored synclines, narrow anticlines and mainly north-westward verging thrusts. These structures, especially the folds, can extend over a length of 200 km. At the periphery, this fold and thrust system is unconformably overlain by Jurassic deposits sealing the deformation. There still remains a relative topographic high on the craton (the Nepa high), revealing a remnant basement morphology, and a trough (called "Pred-Patom trench"), relic of the ancient Vendian-Palaeozoic foredeep overthrusted by the inner range (Fig. 2).

The second (inner) domain is separated from the first one by a thrust zone, evolving in the north-eastern termination of the arc into a strike-slip fault zone. Topographically, it corresponds to the mountain range and it is composed of several imbricated units. A volcanic and sedimentary melange, partly metamorphosed in greenschist to amphibolite facies (*Condie and Rosen, 1994; Zhao et al., 2002*) and considered as a remnant sliver of the so-called Palaeoproterozoic Akitkan orogenic belt (*Zhao et al., 2002*), marks the south-western front. Outcrops of this unit are scarce, but it is the source of numerous rhyolitic pebbles drained by the tributaries of the Lena River. The north-western front and the arc of Patom correspond to the Mama-Bodaibo Riphean foredeep (Fig. 2). In this zone, Riphean sediments prevail, sometimes simply folded and thrusted, like in the northern part of the arc, and sometimes pervasively metamorphosed, like in the Mama region. Within these inverted basins, a discontinuous stripe of pre-Riphean basement is observed, following the general curved shape of the range. This unit is made up of granites and gneiss. It is in places overlain through a sharp unconformity by the Riphean series, and sometimes thrusts north-westward over the fold belt or the Akitkan unit. In the South and East, the inner range is characterized by metamorphic units and an ophiolitic-oceanic complex belt. *Dobretsov et al. (2003)* distinguish two different belts (Nurundukan and Baikal-Muya), but most authors gather them in the so-called Baikal-Muya ophiolitic belt (*Konnikov, 1991; Konnikov et al., 1993; Belichenko et al., 1994*; Fig. 2). In places, the Baikal-Muya belt is overlain by Vendian-Early Cambrian deposits, and in other places it is intruded by Proterozoic (620 Ma, *Dobretsov et al., 2003*) then Palaeozoic granitic plutons. The latter form the so-called "Angara-Vitim batholith". *Delvaux et al. (1995)* inferred an Ordovician to Devonian age for those granitoids, but isotope data give a younger age of 330-290 Ma (late Carboniferous-early Permian, *Bukharov et al., 1992; Yarmolyuk et al., 2003; Tsygankov et al., 2007*). East of the Baikal-Muya belt, the Archaean basement is also exposed in the Aldan shield region. Finally the inner range is cross-cut by the Cenozoic North Baikal Rift System, which does not appear to follow any ancient discontinuities.

3. SEDIMENTARY RECORD AND GEODYNAMIC EVOLUTION OF THE PATOM REGION

3.1. Riphean: opening of the Palaeo-Asian ocean

The basement of the Siberian craton is composed of Archaean to Palaeoproterozoic crystalline rocks (*Ulmishek, 2001*) and was assembled during the Palaeoproterozoic, between 1.95 and 1.85 Ga, by the collision of several crustal blocks (*Rosen et al., 1994; Pisarevsky and Natapov, 2003*). Then, in the late Mesoproterozoic and early Neoproterozoic, the Siberian platform was part of the Rodinia supercontinent (*Pavlov et al., 2000, 2002; Pisarevsky and Natapov, 2003*) like most of the Earth's continental crust at this time (*Hoffman, 1991*).

The history of the Patom range actually began in the Late Proterozoic, at the end of the Riphean time (1650-650 Ma) with the break-up of Rodinia and the opening of the Palaeo-Asian ocean (*Gladkochub et al., 2007*). Remnants of this Riphean oceanic crust are found in the Baikal-Muya ophiolites belt (*Konnikov, 1991; Dobretsov et al., 1992, 2003; Konnikov et al., 1993; Belichenko et al., 1994*). The oldest ophiolites are dated at 830-900 Ma and *Dobretsov et al. (2003)* proposed an age of 900-950 Ma for the initiation of continental rifting at this place. The rifting and the subsequent passive continental margin evolution are characterized on this south-eastern part of the Siberian platform by the deposition of mainly terrigenous series with carbonate intercalations, unconformably overlying the crystalline basement. An outward (eastward to south-eastward) gradual thickening of the Riphean deposits is described (*Khomentovsky et al., 1972; Pisarevsky and Natapov, 2003*) and is generally associated with a passive margin context.

Early Riphean sediments are not well exposed in the Patom region. Metamorphosed conglomerates, sandstones and iron-bearing rocks of the Mama-Bodaibo region could correspond to the lower Riphean Teptogora group (e.g., *Pisarevsky and Natapov, 2003*). A poorly exposed, uncertain middle Riphean carbonate-clastic formation (the Ballaganakh group) is generally described above it but we could not observe it. The oldest sedimentary formation that we could observe in Patom foreland and highland consists of tillite and diamectite deposits (Zhemkukan formation, Fig. 3), with dark greywackes and mainly quartz and gneiss clasts of glacial origin. This succession presents a regional extension (*Khomentovsky et al., 1985; Khomentovsky and Postnikov, 2001; Sintsov, 2005*) but is not precisely dated. The most important glacial episode occurring at the end of the Riphean time to which we can confidently relate these deposits is the Sturtian global event (around 740 Ma, *Knoll et al., 1995; Khomentovsky, 2002; Goddéris et al., 2003*). However, for *Pokrovskii et al. (2006)*, the diamectites formation of the Patom foreland is rather linked to the Marinoan glacial event (665-635 Ma). Thus, this question remains open. Overlying the tillites, we observed successively in the foreland (Fig. 3): 1) a

tidal sandstones formation (Barakun formation) with hummocky cross stratifications and ripple marks, 2) some dark shales and oolitic sandstones (Valukhtin formation), 3) thin and regular silto-carbonates (Nikol formation), and 4) at the top of Riphean sequence massive limestones with numerous stromatolites and algae (Chencha formation, *Pelechaty, 1998*). Thus, during the end of the Riphean, the general tendency is a transition from littoral to shallow-water environments indicating a marine transgression, which is in agreement with a slowly subsiding passive margin (Fig. 4). In Patom highland, the corresponding sequence is thicker and mainly consists of black shales and flyschs, which plead for the existence of deep margin basin at this place ("Mama-Bodaibo foredeep", *Melnikov et al., 1994*).

3.2. Vendian to Devonian: accretion of microcontinents

At the top of the Riphean sequence and during the Vendian, sedimentation becomes dominantly clastic and reflects the beginning of a regression that can be associated with the development of an active margin. This is corroborated by the age of the youngest ophiolites in the Baikal-Muya belt, which indicate that they were obducted not earlier than 650 Ma, i.e. at the Riphean-Vendian boundary (*Delvaux et al., 1995; Dobretsov et al., 2003*; Fig. 4). In the case of the Patom area, the terrane colliding with the Siberian platform is the Barguzin micro-continent to the southeast (*Belichenko et al., 2006; Gordienko, 2006; Makrygina et al., 2007*). Its northern border corresponds to the Baikal-Muya ophiolites belt and follows the arc of the Patom range. Other terranes could have been accreted before that time, like the Akitkan belt in the western part of the range.

Along the Siberian margin, the Vendian is characterized by the deposition of a thick sedimentary sequence, initially clastic and terrigenous (Zherba Formation, Fig. 3), then mainly carbonated (Tinnaya Formation), in conformity with Riphean deposits. In the Patom highland, post-Riphean sediments are absent or consist of a thick succession of Vendian-Cambrian molasses unconformably overlying Riphean sediments (*Delvaux et al., 1995*), which testifies of a first collision stage and the formation of an associated relief. These molasse deposits are now dipping almost vertically and display a crude bedding-parallel schistosity which is not observed in the overlying Cambrian limestones. Deformation of the vendian molasses might thus result from this early collision stage.

After the first continental accretion stage, the relative convergence between the Siberian platform and the Barguzin microcontinent stopped and deformation migrated southward (*Delvaux et al., 1995*). In the Early-Middle Palaeozoic, island arcs and back-arc basins were amalgamated to the initial collage south of the Patom belt (*Delvaux et al., 1995*), without any recorded deformations in the Patom belt. During the Palaeozoic, carbonate deposits cover the whole outer domain and part of the suture zone (Fig 2). They become more and more massive and display more and more proximal facies (late Vendian and Cambrian). Eventually, continental-detritic beds were deposited during the Early Ordovician. Post Early Ordovician sediments are rare in the Patom area. Silurian and sometimes Devonian deposits exist but only within a few large synclines north of the Patom foreland. Thus, the sedimentation was nearly continuous over a long period extending from Late Vendian to Ordovician, i.e. during almost 200 Ma. The corresponding first order sequence is regressive with progressive filling of the foredeep. During this time, the foreland deposits do not record any significant angular unconformity and are devoid of syn-tectonic sediments like flyschs or molasses. Thus, the early docking of the Barguzin microcontinent in Vendian (*Berzin and Dobretsov, 1994; Delvaux et al., 1995*) as the amalgamation of island arcs in Early Palaeozoic times are only recorded in the inner domain and did not induce significant deformation in the Patom foreland. Consequently, these initial collages can not explain the formation of the external Patom fold and thrust belt, which must result from renewed movements and later accretions.

3.3. Late Palaeozoic: collision and closure of the Palaeo-Asian ocean

Then once again the subduction zone and orogenic activity migrated southward and south-eastward while the Palaeo-Mongol-Okhotsk ocean, initiated within the Mongol-China plate, was opening. The Palaeo-Asian ocean was closed in the Carboniferous by collision of the Kazakhstan, Altai and Mongol blocks in a second accretion stage, which reactivated the northward movement of the Barguzin block and induced folding and thrusting over the Siberian margin. In addition, sedimentation stopped at this time on the craton as well as on the margin or in the foredeep around (*Ulmishek, 2001*; Fig. 4). However, this episode was not precisely dated up to now, because there are no sediments younger than late Silurian- early Devonian in the Patom region. Riphean to Ordovician sediments are intruded in the Bolchoi-Patom region by gabbroic to doleritic sills which are folded with the strata. We

have dated these intrusives using the Ar-Ar method and the youngest age found is 385 ± 3.49 Ma, i.e. Late Devonian. The deformed Late Proterozoic and Palaeozoic sedimentary cover of the Patom foreland was then overlain by Jurassic deposits, with a major angular unconformity which is observed in the North of the Patom foreland and along a few remnant buttes within the fold belt. Finally, the Palaeo-Mongol-Okhotsk ocean closed in the Upper Jurassic (*Delvaux et al., 1995; Gordienko, 2006*), without any apparent consequences on the Patom system.

4. STRUCTURAL ANALYSIS

4.1. The Patom foreland

- Outcrop-scale observations

Folding in the foreland basin displays narrow, squeezed anticlines cored by Late Cambrian limestones and dolomites alternating with wide, flat synclines (Fig. 5A). Synclines are underlined in the topography by the Early Ordovician formation of red continental sandstones, and have sometimes a Siluro-Devonian core. These folds are associated with a low amount of shortening: we did not observe in the field neither imbrication nor duplexes, and the estimated individual fault throws are lower than a hundred meters. The deformation is more important in the northern part of the Patom foreland, where folding is irregular, tighter, often asymmetrical and mainly thrust-related (Fig. 5B).

Field measurements and geological mapping allowed us to determine the direction of folds axes which progressively changes following the shape of the belt from N20°E in the West to N150°E in the North-East. The direction of shortening is thus oriented NW-SE in most of the Patom system and becomes N-S in the North and NE-SW in the NE of the range (Fig. 2). In contrast with this homogeneous curvature of fold axes, we observed in the northernmost part of the fold belt a basement uplift (the Ura Uplift) where Proterozoic sediments are folded along a N20°E-trending axis, i.e., almost perpendicular to the general fold system (N110°E). Field observations indicate that the N20°E folds reworked the N110°E folds and are responsible for the tilting of N110°E fold axes (Fig. 5B). The N20°E folding therefore postdated the main folding of the belt, but we do not have absolute constraints on its age.

Besides folds and thrusts, the Patom foreland displays extensional structures of metric to decametric scales. Along the Bolchoi-Patom River, we observed a succession of tilted blocks delimited by syn-sedimentary normal faults in Late Cambrian formations (Fig. 5C). The depositional sequence attests of an emergence episode coeval with fault activity: dark limestones with stromatolites are overlain by fault breccia, evaporites with anhydrite (mainly) and gypsum, and capped at the top by dolomites and Cambrian-early Ordovician continental red sandstones. Normal faults are oriented ~E-W. These observations evidence a regional extensional event that occurred at the end of Cambrian times. The associated structures were subsequently affected by newly formed thrusts during the main compression stage (Fig. 5C).

Strike slip tectonics is described in the north-eastern termination of the arc (*Sintsov, 2003*), where the main frontal thrust seems to evolve into a right-lateral fault zone. *Delvaux et al. (1995)* also inferred the existence of Early Palaeozoic strike-slip (left-lateral) tectonics along Lake Baikal at the south-westernmost tip of the Patom range from micro-tectonic data. However, in the other regions of Patom, as far as we could observe, there is no evidence of deformations or macro-structures related to strike-slip tectonics, in particular at the vicinity of the south-western front. If such tectonics is actually present, it should have a very limited effect on the foreland structure.

- Micro-tectonic data

Fault slip measurements allowed us to characterize the orientation of the principal stress axes associated with the observed meso-scale structures (Figs. 6 and 7) using the computer-based INVDIR method of *Angelier (1984; 1990)*. Table 1 presents the orientation (trend and plunge) of the three principal stress axes σ_1, σ_2 and σ_3 (with $\sigma_1 \geq \sigma_2 \geq \sigma_3$,) and the Φ ratio ($\Phi=(\sigma_2 - \sigma_3) / (\sigma_1 - \sigma_3)$, such as $1 \geq \Phi \geq 0$). The basic assumptions of the stress tensor inversion method are as follow (Lacombe et al., 2006): (1) the bulk rock is physically homogeneous and isotropic; (2) the rock behaves as a rheologically linear material; (3) displacements on the fault planes are small with respect to their lengths; (4) a tectonic event is characterized by a single homogeneous stress tensor, (5) the slip responsible for the striation occurs in the direction and the sense of the maximum resolved shear stress on each fault plan; and (6) the slips on the fault planes are independent of each other. The measurements have been carried out in sedimentary series of Palaeoproterozoic to Silurian age and in granitic and gneissic rocks. If necessary, i.e. when fault-slip data sets were too complex to be

interpreted with a single stress tensor because of a mechanical incompatibility between fault slips and readily resulted from superimposed tectonic events, homogeneous fault subsets were separated and labelled with A or B suffix. Sorting was done in two ways: (1) at sites where all fault planes are of the same type (e.g., normal faults), they were sorted according to strike (e.g., site X and Y); (2) at sites where two different types of fractures are observed (e.g., normal and strike-slip faults), the two subsets were distinguished. However, probably because of the alteration, the amount of fault planes displaying a well-developed striation is low. We considered both the striated fault planes and the simple joints. When the fault sets were evidently tilted due to post-fracturing folding, as visible when the stress axes lay within the bedding plane, back tilting was performed in order to retrieve their original position.

Conjugate reverse faults are observed in Riphean, Cambrian and Ordovician sediments, and indicate a NW-SE direction of compression in most of the Patom foreland, turning to N-S or NNE-SSW in its northern and easternmost parts (Figs. 6 and 7). In this case, the direction of compression (σ_1) is parallel to the direction of shortening indicated by the fold axes (see section x), suggesting that folding and reverse faulting are coeval and pertain to the same tectonic episode. As suggested by the macro-structures, this episode does not seem to overprint a previous compressional (collisional) event. Indeed, most of the reverse faults display only one visible generation of striae. Normal faulting displays a more complicated pattern with alternating ~N-S and ~E-W directions of extension. Syn-sedimentary normal faults observed in upper Cambrian sediments of the Bolchoi-Patom river are characterized by an ~N-S direction of extension (σ_3), a direction also observed in the foreland, in the upper Cambrian deposits very close to the Vitim mouth (site WP 151). An E-W direction of extension is observed 150 km south of the Vitim mouth (site WP 6a) and in basement units ~150 to 200 km upstream the Vitim river (sites WP 191b and WP 212). We do not have constraints on the relative chronology of both directions of extension. Finally, as for the macro-structures, fault slip measurements do not evidence strike-slip tectonics.

4.2. The northern front and the inner domain

The transition from the foreland basin to the inner range corresponds to a smooth positive topography gradient in the northern part of the Patom range. The style of deformation is homogeneous, with numerous narrow, tight and curved folds. The presence in the prolongation of the

Riphean Vilyui aulacogen (Fig. 2) of the Mama-Bodaibo Riphean-Vendian foredeep, inverted by the first collage stage (Vendian, *Khomentovsky and Postnikov, 2001*), can explain that characteristic. Indeed, the indented shape of the Siberian platform and the basement morphology inherited from early Riphean rifting probably allowed the formation of a wider margin with thicker deposits in this place. Consequently, during continental collision shortening can be accommodated on a large length and strain gradients are low. This foredeep progressively thins on each side of the North Patom arc, reducing to a narrow stripe in the Vitim river area.

Right in front of the main thrust, sediments show evidence for ductile deformation. Figure 8A (Bolchoi-Patom river, northern area) shows Late Riphean carbonates of the Nikol formation with boudinage, ductile shearing, ductile folds and schistosity. A similar example was observed in sandstones and quartzites of the Barakun formation (Vitim river, north-western area). The corresponding direction of compression trends N-S in North Patom and SE-NW in NW Patom. Ductile folds are often asymmetric and indicate a frontward direction of transport.

In the inner parts of the range, the deformation is more intense. Along the Vitim River, the basement consists of granites and gneisses. Gneiss units display a low-dipping metamorphic foliation bearing a very homogeneous NW-SE stretching lineation (Fig. 8B). A top-to-the-northwest sense of shear is generally observed in shear bands. Both granites and gneisses are also affected by brittle faulting, indicating a direction of compression similar to these observed in the foreland domain.

Metapelite units are observed along the Vitim River, between Mama and Vitimsky. From the literature, it is possible that these metamorphosed sediments correspond to lower Riphean clastic rocks of the Teptogora group (*Sharov et al., 1991; Pisarevsky and Natapov, 2003*). These rocks display a metamorphic foliation trending N20°E to N70°E and gently dipping toward the south-east. Deformed markers attest of an important shortening, like for instance the isoclinal folding of quartz veins (Fig. 8C).The metamorphic lineation displays a very homogeneous NW-SE trend. Shear bands of centimetric to decametric size, asymmetric boudinage, pressure shadows around garnets, or ductile folds, consistently indicate a top-to-the-North-West sense of shear (Fig. 8C). This deformation is similar to that observed in the gneiss units. Thin sections carried out on collected samples following the lineation axis (XZ plane of finite strain, Fig. 9) show microstructures which confirm the macroscopic observations: south-eastward dipping foliation and top-to-the-North-West shearing (Figs. 9a and 9b). On the other hand, observed parageneses indicate conditions corresponding to the amphibolite facies.

Thin section in Figure 9a (sample PA0660) shows assemblage of garnet, kyanite, biotite, muscovite and plagioclase phases which is typical of the observed peak metamorphism conditions in this metamorphic belt. Such a paragenesis and the absence of melting (e.g. migmatites) allows us to estimate the peak conditions (Fig. 9c), according to the average pelite composition and equilibria in the NCKFMASH system proposed by *White et al., 2001*. Refined estimation using microprobe analysis on sample PA0660 (Table 2) and equilibrium computation using the THERMOCALC software (*Holland and Powell, 1998*) gave a maximum P-T estimate of 10 kbar and 700 °C.

In every units of the Patom range, deformations follow a very consistent scheme with a W to N vergency, following the curved shape of the range. This result seems to indicate a single-phased structuration of the fold and thrust belt which is consistent with the relatively simple and slow evolution of the sedimentary context. However, in spite of the structural consistence between foreland and inner units, the relatively high metamorphic grade described above makes unclear the internal-external tectonic relationships. Indeed, the assumed peak conditions reached in the metamorphic belt strongly contrast with the weak amounts of strain accommodated in the foreland. Moreover, the gradient observed across the frontal thrust, as the morphology, is smooth in the northern part of the range, and high at the western front. The initial indented shape of the Siberian craton's margin (inherited from Riphean rifting), its rigidity and a probably very narrow and steep margin West of the Patom arc may explain this contrast.

4.3. Regional-scale cross sections

The available geological information (1/500.000 geological map, *Kuznetsov et al., 1982*) and field observations (strata dips, faults) are synthesized in three cross-sections of regional scale representing the north, centre, and the south of the range (Fig. 10). The first-order basement topography is deduced from isobaths maps (not publishable), interpreted after gravimetry and magnetic data. But except for a few boreholes, no other data (seismic or geophysical) are available concerning the overlying cover. Consequently, the level of detail presented here is limited. The balancing rules have been respected for these sections. Based on the fold wavelength and on the assumed thickness of the sedimentary sequence, we propose that the basal decollement level lies in the diamectites of the Zhemkukan formation, i.e. at the base of the upper Riphean.

The southern section (A-A') presents a rather thick-skin tectonic style. Most of the deformation in the foreland is boxed by basement faults cross-cutting the cover and corresponding to structural steps. The sedimentary cover in the foreland domain is almost undeformed, except the Late Cambrian-Ordovician series which are sometimes folded and thrusted on thin Late Cambrian decollement (see Fig. 3). The transition with the inner range is marked by an abrupt topographic step and by a large strain gradient: deformation in the inner range is very intense, and the basement is directly thrusting over the foreland on a single main thrust. Conversely, in the Vitim (section B-B') and North (section C-C'-C'') of Patom areas, the tectonic style is dominantly thin-skin. The main faults of the foreland sole into deep decollements (Riphean levels in the trench and infra-Cambrian above the Nepa high). Compared to the south, the sedimentary cover is more deformed (especially in the northern arc), and there is no single basement / foreland main thrust. The "fold and thrust belt" consists in a succession of narrow anticlines alternating with large and almost flat synclines. Anticlines lie above a thin and shallow decollement level and are generally associated with east or southeast-vergent thrusts (Fig. 5A). Finally, the topographic transition between the basin and the high range is not as abrupt as in the south, and the mean topographic slope of the foreland basin is close to zero, sometimes even negative.

The three sections evidence a progressive thickening of the sedimentary cover from the Nepa High to the Pred-Patom trench. The older are the deposits, the more the thickening is obvious. This wedge geometry corresponds to that of a passive margin during the Riphean and subsequently to the foredeep basin developed during the Vendian-Palaeozoic collision stage. As a consequence of the south-eastward thickening of the sedimentary cover, folds have a larger wavelength in the Pred-Patom trench than in the Nepa High. Thickness variations are also observed laterally, along the strike of the Patom range (up to 7000 meters of sediments in the North, no more than 3500 meters in the South). The Proterozoic sequence, which is very thick in the North, becomes progressively thinner toward the South and disappears along the southern section.

The thrust faults are mainly front-verging, and some of them have a large dip angle and probably correspond to reactivated ancient normal faults inherited from Riphean rifting. The three sections advocate for a low amount of shortening, mainly accommodated at the frontal zone, i.e. along one single or several thrusts which are associated with topographic gradients or steps. Thus, there is no typical foreland wedge associated to the Patom range.

In addition to these sections, we propose a simplified N-S interpretation transect of the inner parts of the Patom range. This section is unbalanced, not constrained by geophysical data but summarizes field structural observations on the scale of the whole range. Figure 11 shows from South to North (see section 2 for description of the units): the Muya basin (part of the active North Baikal Rift System); the ophiolitic units thrusting the Riphean deposits and the Proterozoic basement; Vendian syntectonic sequence (especially conglomerates) and Cambrian carbonates; the Angara-Vitim Batholith; the Mama-Bodaibo foredeep, filled by Riphean flysches and inverted at the Riphean-Vendian transition; the north-eastern frontal zone, probably accommodating the largest part of the shortening; and the Patom foreland, with moderate folding. This interpretation support the chronology presented in section 3 for the geodynamic evolution of the Patom region.

5. CONCLUSION - DISCUSSION

Field data allowed us to draw the chronology of the main tectonic phases recorded in the study region (Figs. 4 and 12). The upper Cambrian is marked by a phase of tectonic extension that is observed in different parts of the foreland domain with either N-S or E-W direction, associated with typical syn-tectonic sedimentary sequences (Fig. 5C.). Up to now, this phase was not described in the surrounding region, and it is difficult to associate it with a major tectonic event. It might correspond to a phase of stress relaxation following the Vendian collision. The main compressional episode responsible for the development of fold and thrusts in the foreland and outer range and metamorphism and ductile deformation in the inner range is clearly posterior to the youngest outcropping deposits, i.e., post-Silurian. It also reworks Cambrian tilted blocs whose horsts are cross-cut on their top by numerous subsequent reverse faults. The age of this phase can be bracketed between the Late Devonian corresponding to the age of folded sills and the Carboniferous post-orogenic granitoid intrusions (*Bukharov et al., 1992; Yarmolyuk et al., 2003; Tsygankov et al., 2007*). This compression could correspond to one of the four Palaeozoic deformation stages described in the Baikal region by *Delvaux et al. (1995)*.

Finally, another phase of compression is recorded locally in the corridor of N20°E folds located in the NE part of the Patom range; here again, no precise constraints can be given concerning its absolute age, but field data indicate that it is clearly posterior to the former.

Except the Cambrian extension, our field data are consistent with previous studies and advocate for a rather simple stratigraphic and tectonic history. The first-order stratigraphic sequence is made of a long (considering the whole Late Riphean) transgressive period followed by a quite as long regression (from Vendian until at least Ordovician), with only one regional unconformity in between. Tectonic data, although sampled in formations of different ages and structural styles, describe a very uniform direction of compression between the range and the foreland basin. Metamorphic foliations and lineations, the tight folds with schistosity and boudinage, and the long-wavelength outermost folds therefore appear to have formed during the same tectonic stage. Moreover, it is consistent with the conclusions obtained by stress-strain field modelling (*Sintsov 2003*), which indicate a formation of the Patom belt under uniaxial N-S compression and southward motion of the Siberian platform (or northward motion of the Barguzin block) in present-day coordinates.

Variations in the amount of strain, structural style and direction of structures can be explained by the initial indented shape of the Siberian craton's margin inherited from Riphean rifting: West and East of the Patom arc, the margin was probably very narrow and steep (possibly transform) and accumulated a thin layer of Riphean sediments. On the other hand, a wide and deep passive margin developed in the central part of the Patom arc with a considerable amount of sediments. During subsequent ~N-S compression, deformation could spread over a long distance and on a thick pile of sediments, including various potential decollement levels in the central domain, whereas it was constrained to narrow stripes west and east of it because the cratonic margin acted as a steep rigid backstop. As a consequence, the total finite strain is lower in the central domain because shortening is distributed over a longer distance. The curved shape of the Patom range is likely due to progressive warping of initially E-W fold axes into this weaker central domain.

The presence of a pre-existing basement morphology can also explain the different tectonic styles shown in the cross sections. First, the basement/cover ratio is higher south of the Patom system, where the margin sedimentation is less developed. Second, Riphean decollement levels cannot work in the south of the foreland because the Proterozoic is missing.

The shape of cratonic keels as it is acquired during the early stages of their history plays a determinant role in the development of pericratonic ranges during subsequent collage episodes. In the Palaeozoic, cratonic keels were almost as rigid as today because thermal gradients have already reached their steady-state (*e.g., Burov and Diament, 1995*). During continental accretions that result in very large continental areas like Eurasia, the presence of cratons must control the localisation and timing of deformation: steep cratonic margins prevent strain propagation in the foreland domain and favour a strong localisation in the narrow marginal domain, whereas a low-dipping margin with large sediment thickness promotes a distributed deformation. In any case, amounts of strain are low and cratonic keels prevent the development of crustal-scale thrusts and the associated ranges mainly consist of a more or less wide basin squeezed against a rigid indentor. As deformation can hardly propagate in the cratonic domain, it stops rapidly and migrates behind the accreted continental block.

ACKNOWLEDGMENTS

This work has been supported by TOTAL S.A. The authors would like to thank the Institute of the Earth Crust (Irkutsk, Russia) for its support for fieldwork. The authors are grateful to reviewers (Karel Schulmann and anonymous), Onno Oncken (editor) and Matthew Dailey (editor's assistant).

REFERENCES

Angelier, J. (1984), Tectonic analysis of fault slip data sets. *J. Geophys. Res.,* **89**, 5835-5848.

Angelier, J. (1990), Inversion of field data in fault tectonics to obtain the regional stress - III. A new rapid direct inversion method by analytical means, *Geophysical Journal International*, *103*, 363-376.

Belichenko, V. G., N. K. Geletii, and I. G. Barash (2006), Barguzin Microcontinent (Baikal mountain area): the problem of outlining, *Russian Geology and Geophysics*, *47*, 1045-1055.

Belichenko, V. G., E. V. Sklyarov, N. L. Dobretsov, and O. Tomurtogoo (1994), Geodynamic map of the Paleo-Asian ocean (eastern part), *Russian Geology and Geophysics*, *35*, 29-40 (Russian version).

Berzin, N. A., and N. L. Dobretsov (1994), Geodynamic evolution of Southern Siberia in Late Precambrian-Early Paleozoic time, in *Reconstruction of the Paleo-Asian Ocean* edited by R. G. Coleman, pp 45-62, VSP Int. Sci. Publishers, Netherlands.

Buchan, C., J. Pfander, A. Kröner, T. S. Brewer, O. Tomurtogoo, D. Tomurhuu, W. D. Cunningham, and B. F. Windley (2002), Timing of accretion and collisional deformation in the Central Asian Orogenic Belt: implications of granite geochronology in the Bayankhongor Ophiolite Zone, *Chemical Geology*, *192*, 23-45.

Bukharov, A. A., V. A. Khalilov, T. M. Strakhova, and V. V. Chernikov (1992), Geology of the Baikal-Patom Upland according to new data of U-Pb dating of accessory zircon, *Russian Geology and Geophysics*, *33*, 24–33.

Burov, E. B., and M. Diament (1995), The effective elastic thickness (Te) of continental lithosphere: What does it really mean ?, *Journal of Geophysical Research*, *100*, 3905-3927.

Condie, K. C., and O. M. Rosen (1994), Laurentia–Siberia connection revisited, *Geology*, *22*, 168-170.

Coney, P. J., D. L. Jones, and J. W. H. Monger (1980), Cordilleran suspect terranes, *Nature*, *288*, 329-333.

Delvaux, D., R. Moeys, G. Stapel, A. Melnikov, and V. Ermikov (1995), Palaeostress reconstructions and geodynamics of the Baikal region, Central Asia, part I. Palaeozoic an Mesozoic pre-rift evolution, *Tectonophysics*, *252*, 61-101.

Dobretsov, N. L., M. M. Buslov, and V. A. Vernikovsky (2003), Neoproterozoic to early Ordovician evolution of the Paleo-Asian ocean : implications to the break-up of Rodinia, *Gondwana Research*, *6*, 143-159.

Dobretsov, N. L., E. G. Konnikov, and N. N. Dobretsov (1992), Precambrian ophiolite belts of southern Siberia, Russia and their metallogeny, *Precambrian Research*, *58*, 427-446.

English, J. M., and S. T. Johnston (2005), Collisional orogenesis in the northern Canadian Cordillera: Implications for Cordilleran crustal structure, ophiolite emplacement, continental growth, and the terrane hypothesis, *Earth and Planetary Science Letters*, *232*, 333-344.

Gladkochub, D. P., T. V. Donskaya, A. M. Mazukabzov, A. M. Stanevich, E. V. Sklyarov, and V. A. Ponomarchuk (2007), Signature of Precambrian extension events in the southern Siberian craton, *Russian Geology and Geophysics*, *48*, 17-31.

Godderis, Y., Y. Donnadieu, A. Nedelec, B. Dupre, C. Dessert, A. Grard, G. Ramstein, and L. M. Francois (2003), The Sturtian 'snowball' glaciation: fire and ice, *Earth and Planetary Science Letters*, *211*, 1-12.

Gordienko, I. V. (2006), Geodynamic evolution of late Baikalides and paleozoids in the folded periphery of the Siberian craton, *Russian Geology and Geophysics*, *47*, 53-70.

Helo, C., E. Hegner, A. Kroner, G. Badarch, O. Tomurtogoo, B. F. Windley, and P. Dulski (2006), Geochemical signature of Paleozoic accretionary complexes of the Central Asian Orogenic Belt in South Mongolia: Constraints on arc environments and crustal growth, *Chemical Geology*, *227*, 236-257.

Hoffman, P. F. (1991), Did the breakout of Laurentia turn Gondwana inside out?, *Science*, *252*, 1409-1412.

Holland, T. J. B., and R. Powell (1998), An internally consistent thermodynamic data set for phases of petrological interest, *Journal of Metamorphic Geology*, *16*, 309-472.

Johnston, S. T., and G. D. Borel (2007), The odyssey of the Cache Creek terrane, Canadian Cordillera: Implications for accretionary orogens, tectonic setting of Panthalassa, the Pacific superwell, and break-up of Pangea, *Earth and Planetary Science Letters*, *253*, 415-428.

Khain, E. V., E. V. Bibikova, E. B. Salnikova, A. Kroner, A. S. Gibsher, A. N. Didenko, K. E. Degtyarev, and A. A. Fedotova (2003), The Palaeo-Asian ocean in the Neoproterozoic and early Palaeozoic: new geochronologic data and palaeotectonic reconstructions, *Precambrian Research*, *122*, 329-358.

Khomentovsky, V. V. (2002), Baikalian of Siberia (850–650 Ma), *Russian Geology and Geophysics*, *43*, 313-333.

Khomentovsky, V. V., and A. A. Postnikov (2001), Neoproterozoic Evolution of the Baikal-Vilyui Branch of the Paleoasian Ocean, *Geotectonics*, *35*, 149-164.

Khomentovsky, V. V., V. Y. Shenfil', and M. S. Yakshin (1985), The Riphean of the Siberian Craton, *Russian Geology and Geophysics*, *7*, 25-33.

Khomentovsky, V. V., V. Y. Shenfil', M. S. Yakshin, and E. P. Butakov (1972), Reference sections of deposits of Upper Precambrian and Lower Cambrian of Siberian Platform, Nauka, Moscow (in Russian).

Knoll, A. H., J. P. Grotzinger, A. J. Kaufman, and P. Kolosov (1995), Integrated approaches to terminal Proterozoic stratigraphy : an example from the Olenek Uplift, northeastern Siberia, *Precambrian Research*, *73*, 251-270.

Konnikov, E. G. (1991), On the problem of ophiolites of the Baikal-Muya belt, *Sov. Geol. Geophys.*, *32*, 104-113.

Konnikov, E. G., A. S. Gibsher, A. E. Izokh, E. V. Sklyarov, and E. V. Khain (1993), Paleogeodynamics of Late Precambrian for Baikal-Muya and Sayat-Tuva-Mongolia segments of the Central Asian fold belt, in *Proceedings of the 4th International Symposium of IGCP Project 283: Geodynamic Evolution of the Paleo-Asian Ocean*, Novosibirsk, 15-24 June, 88-90.

Kröner, A., B. F. Windley, G. Badarch, O. Tomurtogoo, E. Hegner, D. Y. Liu, and M. T. D. Wingate (2005), Accretionary growth in the Central Asian Orogenic Belt of Mongolia during the Neoproterozoic and Palaeozoic and comparison with the Arabian-Nubian Shield and the present Southwest Pacific, *Geophysical Research Abstracts*, *Vol. 7*, 06650.

Kuznetsov, V. G., P. M. Khrenov et al. (1982), Geologicheskaya karta, Irkutskoi oblasti i sopredel'n'ikh territorii, 1:500.000, *Ministerstvo Geologii SSSR*.

Lacombe, O., F. Mouthereau, S. Kargar, and B. Meyer (2006), Late Cenozoic and modern stress fields in the western Fars (Iran): implications for the tectonic and kinematic evolution of central Zagros, *Tectonics*, *25*, TC1003, doi:10.1029/2005TC001831.

Makrygina, V. A., V. G. Belichenko, and L. Z. Reznitsky (2007), Types of paleoisland arcs and back-arc basins in the northeast of the Paleoasian Ocean (from geochemical data), *Russian Geology and Geophysics*, *48*, 107-119.

Melnikov, A. I., A. M. Mazukabzov, E. V. Sklyarov, and E. P. Vasiliev (1994), Baikal rift basement: structure and tectonic evolution, *Bull. Centr. Rech. Explor. Prod. Elf Aquitaine*, *18*, 99- 122.

Monger, J. W. H. (1997), Plate tectonics and northern Cordilleran geology: an unfinished revolution, *Geoscience Canada*, *24*, 189-198.

Pavlov, V. E., Y. Gallet, P. Y. Petrov, D. Z. Zhuravlev, and A. V. Shatsillo (2002), The Ui Group and Late Riphean Sills in the Uchur–Maya Area: Isotope and Paleomagnetic Data and the Problem of the Rodinia Supercontinent, *Geotectonics*, *36*, 278-292.

Pavlov, V. E., Y. Gallet, and A. V. Shatsillo (2000), Paleomagnetism of the Upper Riphean Lakhandinskaya Group in the Uchuro-Maiskii Area and the Hypothesis of the Late Proterozoic Supercontinent, *Izvestiya, Physics of the Solid Earth*, *36*, 638-648.

Pelechaty, S. M. (1998), Integrated chronostratigraphy of the Vendian System of Siberia: implications for a global stratigraphy, *Journal of the Geological Society, London*, *155*, 957-973.

Pisarevsky, S. A., and L. M. Natapov (2003), Siberia and Rodinia, *Tectonophysics*, *375*, 221-245.

Pokrovskii, B. G., V. A. Melezhik, and M. I. Bujakaite (2006a), Carbon, Oxygen, Strontium, and Sulfur Isotopic Compositions in Late Precambrian Rocks of the Patom Complex, Central Siberia: Communication 1. Results, Isotope Stratigraphy, and Dating Problems, *Lithology and mineral ressources*, *41*, 450-474.

Pokrovskii, B. G., V. A. Melezhik, and M. I. Bujakaite (2006b), Carbon, Oxygen, Strontium, and Sulfur Isotopic Compositions in Late Precambrian Rocks of the Patom Complex, Central Siberia: Communication 2. Nature of Carbonates with Ultralow and Ultrahigh $d^{13}C$ Values, *Lithology and mineral ressources*, *41*, 576-587.

Pubellier, M., F. Ego, N. Chamot-Rooke, and C. Rangin (2003), The building of pericratonic mountain ranges : structural and kinematic constraints applied to GIS-based reconstructions of SE Asia, *Bull. Soc. géol. Fr.*, *174*, 561-584.

Rosen, O. M., K. C. Condie, L. M. Natapov, and A. D. Nozhkin (1994), Archean and Early Proterozoic evolution of the Siberian craton: a preliminary assessment, in *Archean Crustal Evolution*, edited by K. C. Condie, 411-459, Elsevier, Amsterdam.

Sengör, A. M. C., B. A. Natal'in, and V. S. Burtman (1993), Evolution of the Altaid tectonic collage and Palaeozoic crustal growth in Eurasia, *Nature*, *364*, 299-307.

Sharov, V. N., N. I. Fefelov, N. V. Zarudnova, V. A. Rusakova, and S. B. Brandt (1991), Pb-Pb dating of the Mama synclinorium schists: Patom highland. *Dokl. Akad. Nauk SSSR 319*, 209-212 (in Russian).

Sintsov, A. V. (2003), The structure and stress-strain field of the Baikal-patom foldbelt: implications for origins, *Russian Geology and Geophysics*, *44*, 919-928.

Sintsov, A. V. (2005), Structura-Vieschiestviennie complexe Baikalo-patomskoye skladchatoy dugui y correlatsia geologitcheski sobuiti vie vniechniei y vnutrenniei zona, *Stratigraphia y geologicheskaya correlatsia*, *13*, 48-60 (in Russian).

Tsygankov, A. A., D. I. Matukov, N. G. Berezhnaya, A. N. Larionov, V. F. Posokhov, B. T. Tsyrenov, A. A. Khromov, and S. A. Sergeev (2007), Late Paleozoic granitoids of western Transbaikalia: magma sources and stages of formation, *Russian Geology and Geophysics*, *48*, 120-140.

Ulmishek, G. F. (2001), Petroleum Geology and Resources of the Nepa-Botuoba High, Angara-Lena Terrace, and Cis-Patom Foredeep, Southeastern Siberian Craton, Russia, *U.S. Geological Survey Bulletin*, *2201-C*.

White, R. W., R. Powell and T. J. B. Holland (2001), Calculation of partial melting equilibria in the system Na2O-CaO-K2O-FeO-MgO-Al2O3-SiO2-H2O (NCKFMASH), *J. metamorphic Geology, 19*, 139-153.

Windley, B. F., D. Alexeiev, W. J. Xiao, A. Kröner, and G. Badarch (2007), Tectonic models for accretion of the Central Asian Orogenic Belt, *J. Geo. Soc. London*, *164*, 31-47.

Yarmolyuk, V. V., and V. I. Kovalenko (2003), Batholiths and geodynamics of batholith formation in the Central Asian fold belt, *Russian Geology and Geophysics*, *44*, 1305-1320.

Zhao, G., P. A. Cawood, S. A. Wilde, and M. Sun (2002), Review of global 2.1–1.8 Ga orogens : implications for a pre-Rodinia supercontinent, *Earth-Science Reviews*, *59*, 125-162.

FIGURE CAPTIONS:

Figure 1. **A** - Location of the Patom range, within the Central Asian Orogenic Belt and related to the Siberian craton. **B** - Topography of the studied area from SRTM (Shuttle Radar Topography Mission) digital elevation model (sample spacing of 3 arc-second), itineraries followed for the field survey (solid red, yellow and purple lines), and location of the outcrops or samples presented in Figures 5, 8 and 9.

Figure 2. Sketch map of the Patom fold and thrust belt, after 1/500.000 Russian geological map (*Kuznetsov et al., 1982*) and field observations.

Figure 3. **A** - Main identified sedimentary domains in the Patom range and foreland (I: Nepa High and external foreland; II: Pred-Patom trench and northern frontal zone; III: Mama-Bodaibo foredeep and western frontal zone; IV: suture zone). **B** - Synthetic stratigraphic logs established and correlated for each sedimentary domain after field observations (Zh: Zhemkukan formation; Br: Barakun formation; Vl: Valukhtin formation; Nl: Nikol formation;

Ch: Chencha formation; Zb: Zherba formation; Tn: Tinnaya formation; Nk: Nokhtuisk formation; Tb: Tolbachan formation; MC: Middle Cambrian; LC: Late Cambrian; Uk: Ust-Kut formation). **C** - Synthetic stratigraphic log, compiled from field observations in the Patom foreland.

Figure 4. Geodynamic evolution of the extended Patom area (after *Gordienko, 2006*).

Figure 5. **A** - Typical anticlinal folds and thrusts of the foreland basin (late Cambrian carbonates, Lena River, see location on Figure 1B). **B** - 2 stages of deformation in late Riphean sandstones (Barakun formation, Bolchoi-Patom River, see location on Figure 1B). Folds and thrusts consistent with the arcuate belt (b, front view of the outcrop), tilted by the N20°E folding (a, lateral view). **C** - Normal faults and associated tilted blocks (a and b), short-cut by the main compression stage (c), Bolchoi-Patom River (see location on Figure 1B).

Figure 6. Fold axis, strata, schistosity and faults slip measurements, and computed palaeostress directions in the Patom fold and thrust belt: outcrop position and fault slickenside sets. Stereoplots are Schmidt projections, lower hemisphere (N is geographic North and M is magnetic North). Fault planes are shown as thin lines, slickenside lineations (striae) are small dots with single (reverse or normal slip) or double (strike slip) thin arrows. Three, four and five-branch stars are computed axes σ_3, σ_2 and σ_1 respectively. Large arrows are directions of horizontal extension and compression (black: calculated, white: inferred).

Figure 7. Computed horizontal palaeostress directions in the Patom fold and thrust belt: stress regimes and corresponding outcrop ages. Large arrows are directions of horizontal extension and compression (black: calculated, white: inferred).

Figure 8. **A** - Ductile deformation of late Riphean carbonates (Nikol formation, Bolchoi-Patom River, see location on Figure 1B). a : boudinage and shearing; b : ductile folds; c : similar folds. **B** - Example of metamorphic foliation (a) and lineations (b, c and d) in the gneiss of the basement units (Vitim River, see location on Figure 1B). **C** - Ductile deformation in the metamorphic units (Vitim River, see location on Figure 1B). a : strong isoclinal folding of a quartz vein; b : boudinage and shearing of quartz vein; c : shear band.

Figure 9. **a** and **b** - thin sections of metamorphic rocks samples and main observed mineral phases. **c** - *P-T* pseudosection for an average pelite composition in the NCKFMASH system, after

White et al., 2001, and estimated peak metamorphism conditions for the metamorphic belt of Patom.

Figure 10. Proposed cross-sections of the Patom foreland, after Russian geological map *(Kuznetsov et al*., 1982) and field observations.

Figure 11. Proposed simplified cross-section of the Patom range, after Russian geological map (*Kuznetsov et al., 1982*) and field observations.

Figure 12. Chronology of the main events occurring in the Patom region.

Table 1. Trend and plunge of principal stress axes computed from fault slip data.

Table 1. Trend and plunge of Principal Stress Axes Computed From Fault Slip Data

Site	Latitude N (°)	Longitude E (°)	Age of rocks	n	σ_1	σ_2	σ_3	Φ	RUP	α	Q
WP 6a	58°42'16.414"	110°53'45.778"	Late Cambrian	4	190 / 73	351 / 16	082 / 05	0.25	62	1	C
WP 6b	58°42'16.414"	110°53'45.778"	Late Cambrian	4	148 / 07	332 / 83	238 / 01	0.48	34	5	B
WP 6c	58°42'16.414"	110°53'45.778"	Late Cambrian	11	128 / 04	037 / 14	232 / 75	0.22	28	7	A
WP 9	60°00'43.794"	117°08'47.097"	Late Riphean	7	227 / 06	339 / 74	136 / 15	0.52	21	11	B
WP 10b	60°00'08.116"	117°07'26.320"	Late Riphean	3	striated fault planes indicating WNW-ESE compression						
WP 13b*	60°00'42.036"	116°58'21.617"	Late Riphean	8	021 / 01	290 / 34	112 / 56	0.44	62	35	C
WP 38	60°08'53.537"	115°35'49.860"	Late Riphean	4	striated fault planes indicating NNW-SSE compression						
WP 40	60°09'31.605"	115°39'16.128"	Late Riphean	3	striated fault planes indicating NNW-SSE compression						
WP 42*	60°09'23.942"	115°40'44.678"	Vendian	7	268 / 80	017 / 03	107 / 10	0.13	34	4	B
WP 127	60°19'26.624"	116°58'03.078"	Ordovician\Silurian	3	striated fault planes indicating NW-SE compression						
WP 140	60°43'13.625"	115°38'08.589"	Ordovician\Silurian	7	joints indicating NW-SE compression / NE-SW extension						
WP 144	60°20'40.123"	114°18'36.595"	Late Cambrian	16	joints indicating NNE-SSW compression / ESE-WNW extension						
WP 151	59°17'41.815"	112°27'42.643"	Late Cambrian	10	276 / 72	121 / 16	029 / 07	0.55	30	11	A
WP 152	59°16'14.666"	112°24'56.887"	Late Cambrian	11	040 / 02	310 / 12	140 / 78	0.44	26	6	A
WP 153	59°10'31.824"	112°04'13.976"	Late Cambrian	4	153 / 01	063 / 18	247 / 72	0.61	18	3	B
WP 155	59°12'16.263"	111°57'43.742"	Late Cambrian	5	315 / 71	088 / 13	181 / 13	0.37	39	12	A
WP 159	59°12'44.635"	111°57'36.573"	Late Cambrian	4	323 / 01	233 / 03	065 / 87	0.51	17	5	B
WP 160	59°13'34.980"	111°57'36.271"	Late Cambrian	6	292 / 70	101 / 20	192 / 04	0.48	29	9	A
WP 191a	58°31'36.776"	112°54'54.003"	Palaeoproterozoic	18	302 / 01	212 / 03	053 / 86	0.22	29	8	A
WP 191b	58°31'36.776"	112°54'54.003"	Palaeoproterozoic	10	193 / 75	034 / 14	303 / 05	0.73	18	10	B
WP 194	58°28'16.591"	112°51'33.640"	Late Riphean	14	312 / 04	048 / 57	220 / 32	0.18	53	14	B
WP 200	58°23'32.306"	112°49'33.724"	Palaeoproterozoic	4	309 / 08	040 / 09	178 / 78	0.78	14	5	C
WP 203	58°20'07.851"	112°50'51.233"	Palaeoproterozoic	16	313 / 02	043 / 06	201 / 84	0.08	48	13	A
WP 212	58°18'10.915"	112°56'25.739"	Palaeoproterozoic	7	striated fault planes indicating ESE-WNW extension						

From left to right: name of the site shown in Fig. 6 (* calculation made after backtilting); coordinates (latitude and longitude, in degrees); number of fault-slip data used for calculation; σ_1, σ_2, σ_3: maximum, intermediate, and minimum principal stress axes (trend / plunge in degrees); $\Phi = (\sigma_2 - \sigma_3)/(\sigma_1 - \sigma_3)$, ratio of stress differences with $0 \leq \Phi \leq 1$; α: average angle (in degrees) between observed and computed striae, acceptable results for $\alpha < 30°$; RUP: misfit criterion of the INVDIR method (Angelier, 1990), acceptable results for RUP<75%; Q: quality estimator for fault-slip subset and calculated stress tensor (A: good, B: fair, C: poor).

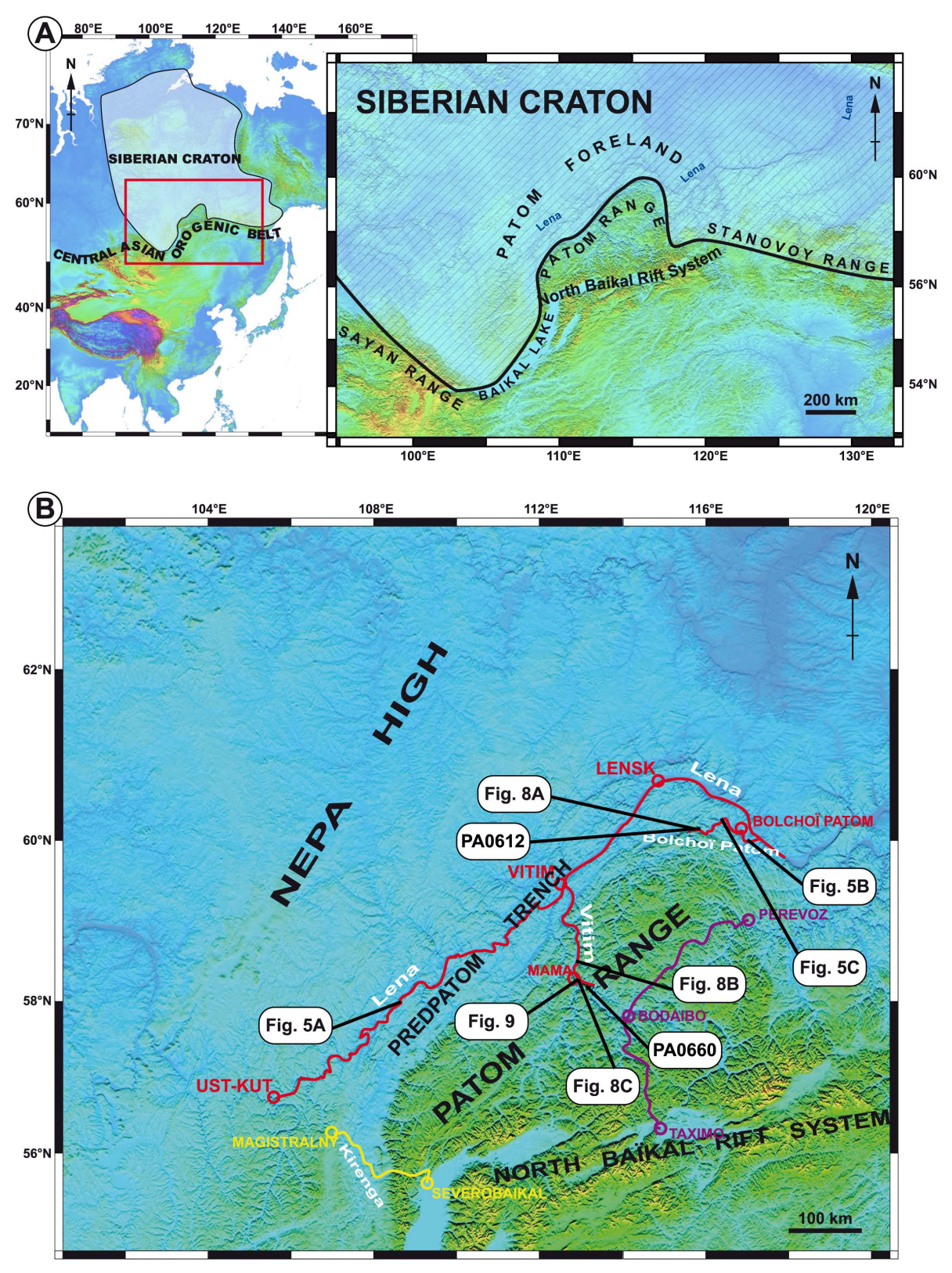
A
80°E
100°E
120°E
140°E
160°E
70°N
60°N
40°N
20°N
N
SIBERIAN CRATON
CENTRAL ASIAN OROGENIC BELT
SIBERIAN CRATON
PATOM FORELAND
PATOM RANGE
STANOVOY RANGE
North Baikal Rift System
BAIKAL LAKE
SAYAN RANGE
Lena
200 km
100°E
110°E
120°E
130°E
60°N
56°N
54°N
B
104°E
108°E
112°E
116°E
120°E
62°N
60°N
58°N
56°N
N
NEPA HIGH
LENSK
Lena
Fig. 8A
PA0612
BOLCHOÏ PATOM
Bolchoï Patom
Fig. 5B
VITIM
TRENCH
Vitim
PEREVOZ
RANGE
Fig. 5C
MAMA
Fig. 8B
Fig. 5A
Lena
PREDPATOM
Fig. 9
BODAIBO
PA0660
PATOM
Fig. 8C
UST-KUT
TAXIMO
MAGISTRALNY
Kirenga
SEVEROBAIKAL
NORTH BAÏKAL RIFT SYSTEM
100 km

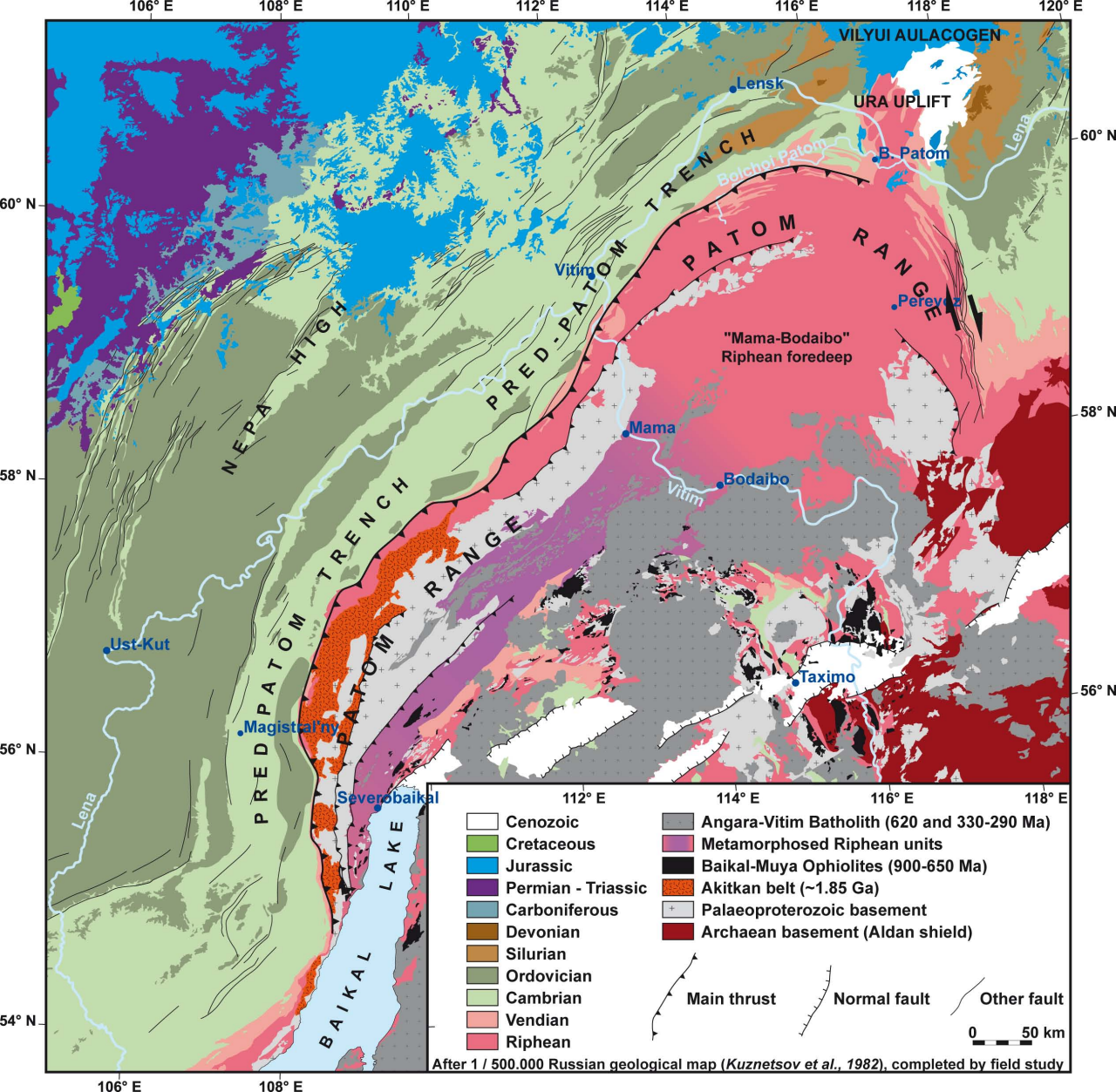
106° E
108° E
110° E
112° E
114° E
116° E
118° E
120° E
60° N
58° N
56° N
54° N
VILYUI AULACOGEN
URA UPLIFT
Lensk
B. Patom
Lena
Bolshoi Patom
Vitim
PATOM RANGE
PRED-PATOM TRENCH
Pereyaz
"Mama-Bodaibo"
Riphean foredeep
Mama
Bodaibo
NEPA HIGH
PREDPATOM TRENCH
PATOM RANGE
Ust-Kut
Magistral'ny
Severobaikal
Taximo
BAIKAL LAKE
Cenozoic
Cretaceous
Jurassic
Permian - Triassic
Carboniferous
Devonian
Silurian
Ordovician
Cambrian
Vendian
Riphean
Angara-Vitim Batholith (620 and 330-290 Ma)
Metamorphosed Riphean units
Baikal-Muya Ophiolites (900-650 Ma)
Akitkan belt (~1.85 Ga)
Palaeoproterozoic basement
Archaean basement (Aldan shield)
Main thrust
Normal fault
Other fault
0 50 km
After 1 / 500.000 Russian geological map (Kuznetsov et al., 1982), completed by field study

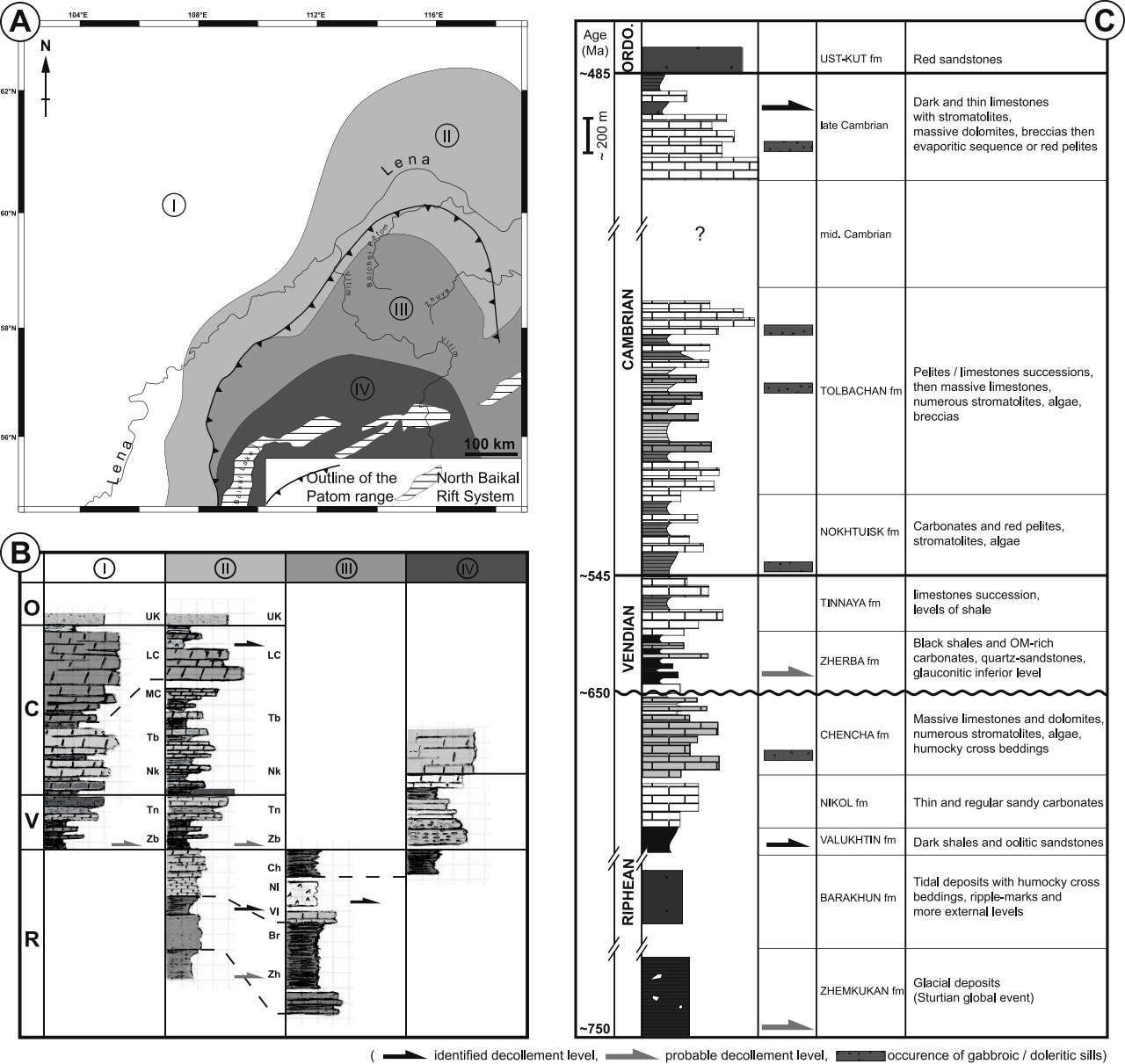
A
104°E
108°E
112°E
116°E
N
62°N
60°N
58°N
56°N
Lena
II
I
III
IV
Lena
Baikal Rift
Zhuya
Ulkan
100 km
Outline of the Patom range
North Baikal Rift System
B
I
II
III
IV
O
C
V
R
UK
LC
MC
Tb
Nk
Tn
Zb
Ch
Nl
Vl
Br
Zh
C
Age (Ma)
ORDO.
CAMBRIAN
VENDIAN
RIPHEAN
~485
~545
~650
~750
~200 m
?
UST-KUT fm
Red sandstones
late Cambrian
Dark and thin limestones with stromatolites, massive dolomites, breccias then evaporitic sequence or red pelites
mid. Cambrian
TOLBACHAN fm
Pelites / limestones successions, then massive limestones, numerous stromatolites, algae, breccias
NOKHTUISK fm
Carbonates and red pelites, stromatolites, algae
TINNAYA fm
limestones succession, levels of shale
ZHERBA fm
Black shales and OM-rich carbonates, quartz-sandstones, glauconitic inferior level
CHENCHA fm
Massive limestones and dolomites, numerous stromatolites, algae, humocky cross beddings
NIKOL fm
Thin and regular sandy carbonates
VALUKHTIN fm
Dark shales and oolitic sandstones
BARAKHUN fm
Tidal deposits with humocky cross beddings, ripple-marks and more external levels
ZHEMKUKAN fm
Glacial deposits (Sturtian global event)
identified decollement level,
probable decollement level,
occurence of gabbroic / doleritic sills)

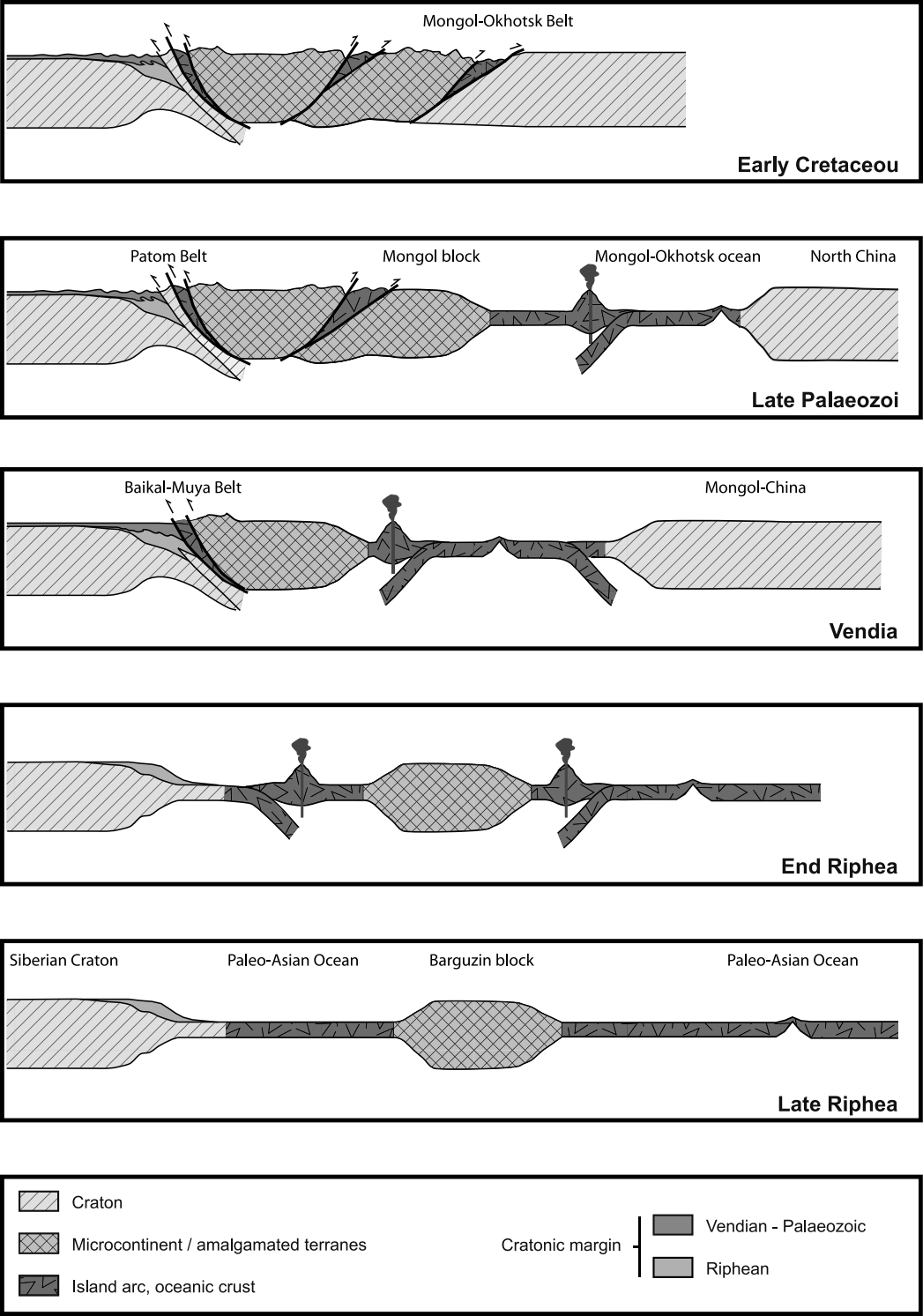
Mongol-Okhotsk Belt
Early Cretaceou
Patom Belt
Mongol block
Mongol-Okhotsk ocean
North China
Late Palaeozoi
Baikal-Muya Belt
Mongol-China
Vendia
End Riphea
Siberian Craton
Paleo-Asian Ocean
Barguzin block
Paleo-Asian Ocean
Late Riphea
Craton
Microcontinent / amalgamated terranes
Island arc, oceanic crust
Cratonic margin
Vendian - Palaeozoic
Riphean

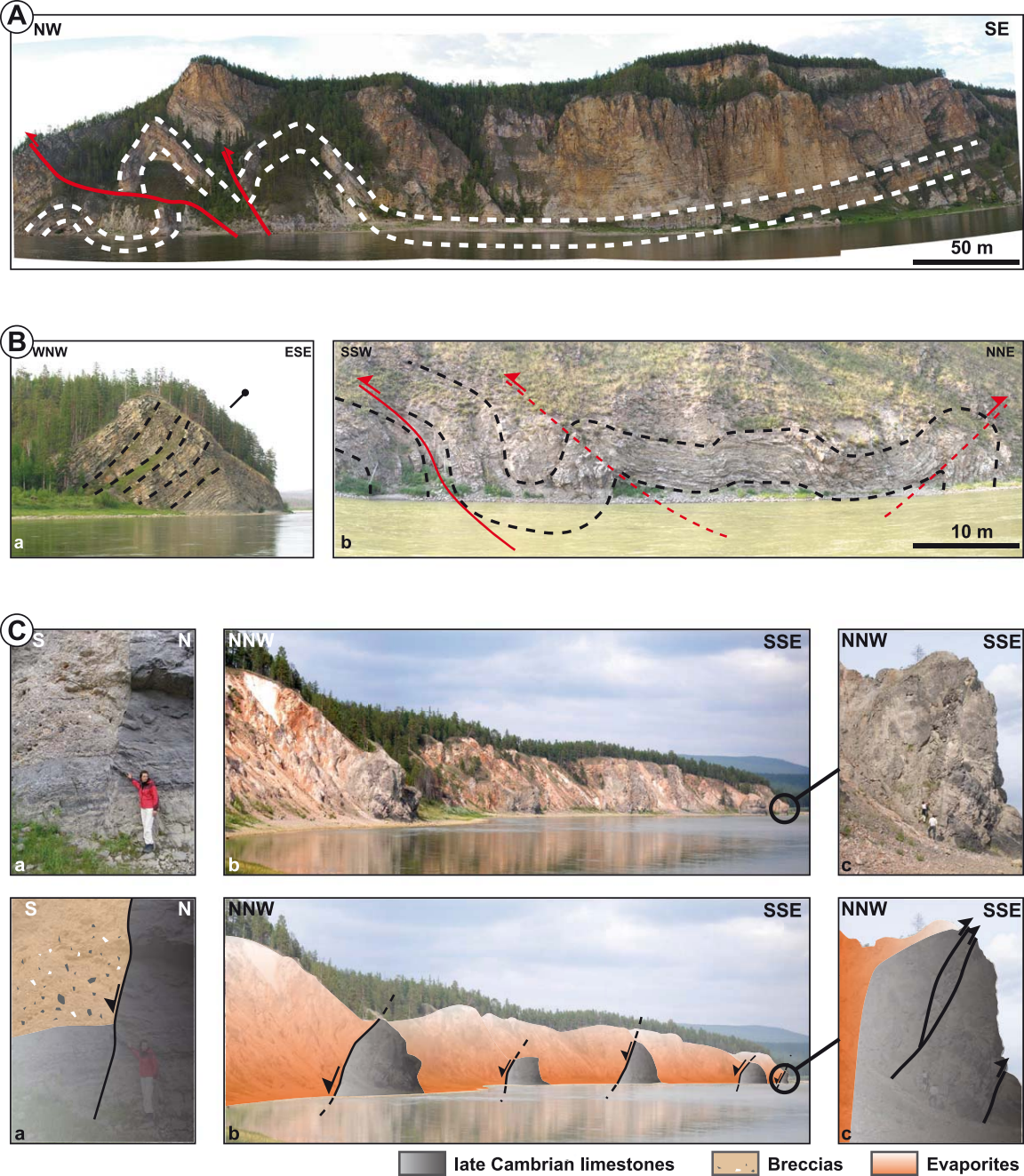
A
NW
SE
50 m
B
WNW
ESE
a
SSW
NNE
b
10 m
C
S
N
a
NNW
SSE
b
NNW
SSE
c
S
N
a
NNW
SSE
b
NNW
SSE
c
late Cambrian limestones
Breccias
Evaporites

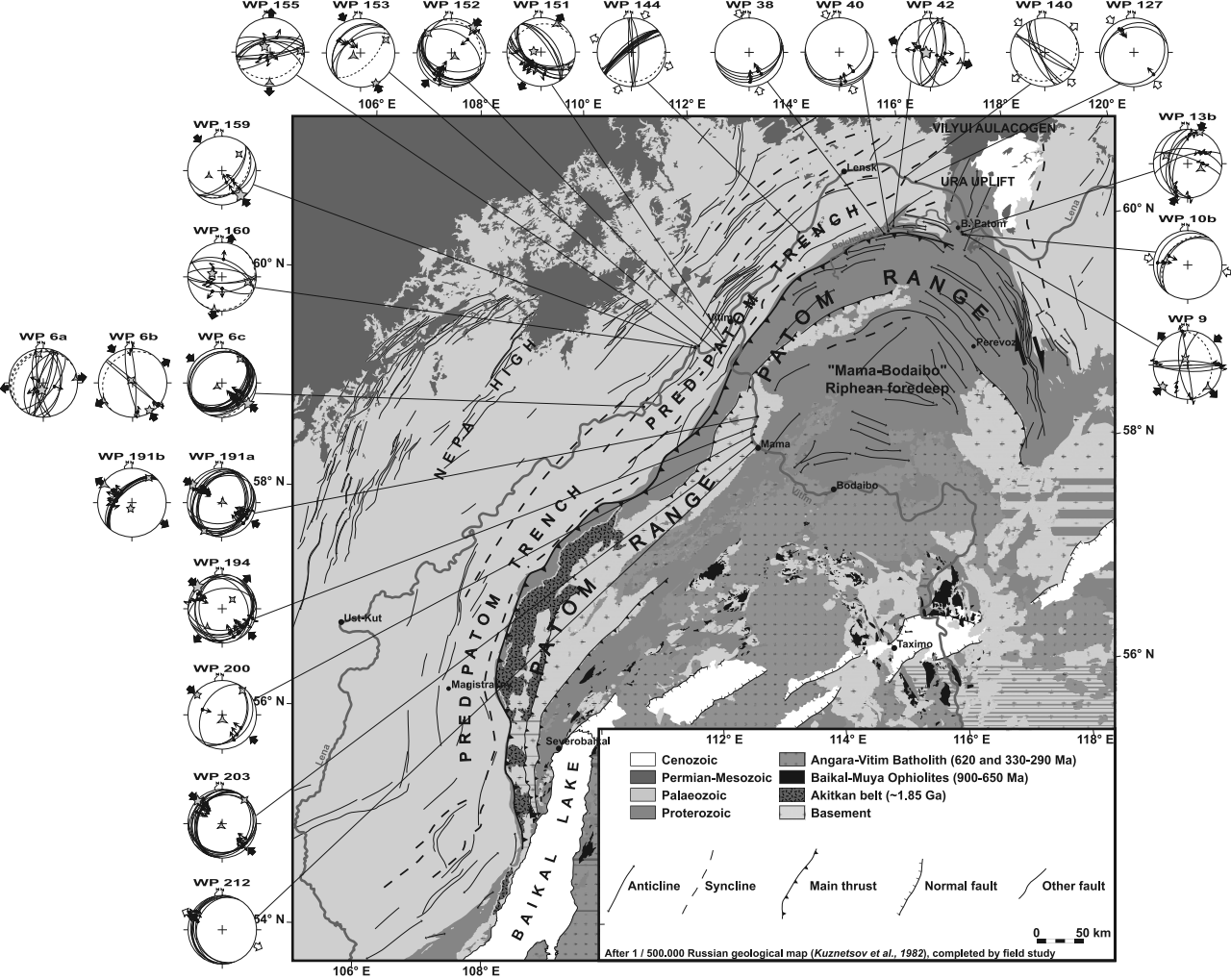
WP 155
WP 153
WP 152
WP 151
WP 144
WP 38
WP 40
WP 42
WP 140
WP 127
WP 159
WP 160
WP 6a
WP 6b
WP 6c
WP 191b
WP 191a
WP 194
WP 200
WP 203
WP 212
WP 13b
WP 10b
WP 9
106° E
108° E
110° E
112° E
114° E
116° E
118° E
120° E
60° N
58° N
56° N
54° N
VILYUI AULACOGEN
URA UPLIFT
Lensk
B. Patom
Lena
Vitim
Rerevoz
"Mama-Bodaibo"
Riphean foredeep
Mama
Bodaibo
Taximo
Ust-Kut
Magistral
Severobaikal
NEPA HIGH
PREDPATOM TRENCH
PATOM RANGE
BAIKAL LAKE
Cenozoic
Permian-Mesozoic
Palaeozoic
Proterozoic
Angara-Vitim Batholith (620 and 330-290 Ma)
Baikal-Muya Ophiolites (900-650 Ma)
Akitkan belt (~1.85 Ga)
Basement
Anticline
Syncline
Main thrust
Normal fault
Other fault
0
50 km
After 1 / 500.000 Russian geological map (Kuznetsov et al., 1982), completed by field study

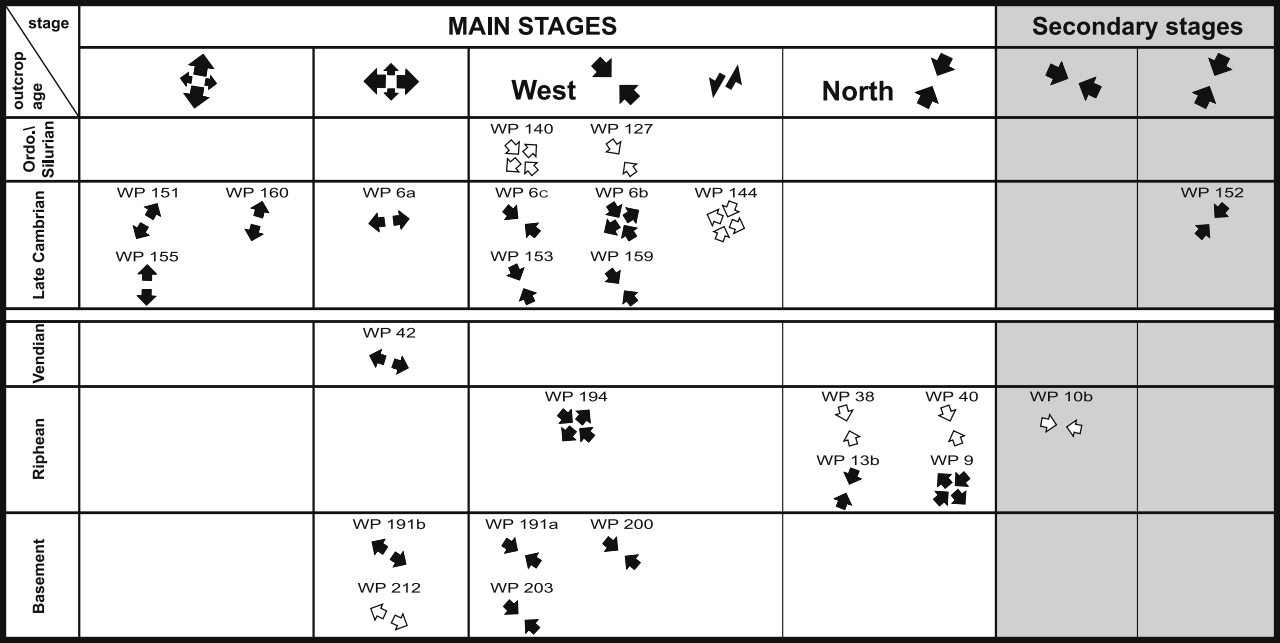
stage
outcrop age
MAIN STAGES
Secondary stages
West
North
Ordo.\ Silurian
Late Cambrian
Vendian
Riphean
Basement
WP 140
WP 127
WP 151
WP 160
WP 6a
WP 6c
WP 6b
WP 144
WP 152
WP 155
WP 153
WP 159
WP 42
WP 194
WP 38
WP 40
WP 10b
WP 13b
WP 9
WP 191b
WP 191a
WP 200
WP 212
WP 203

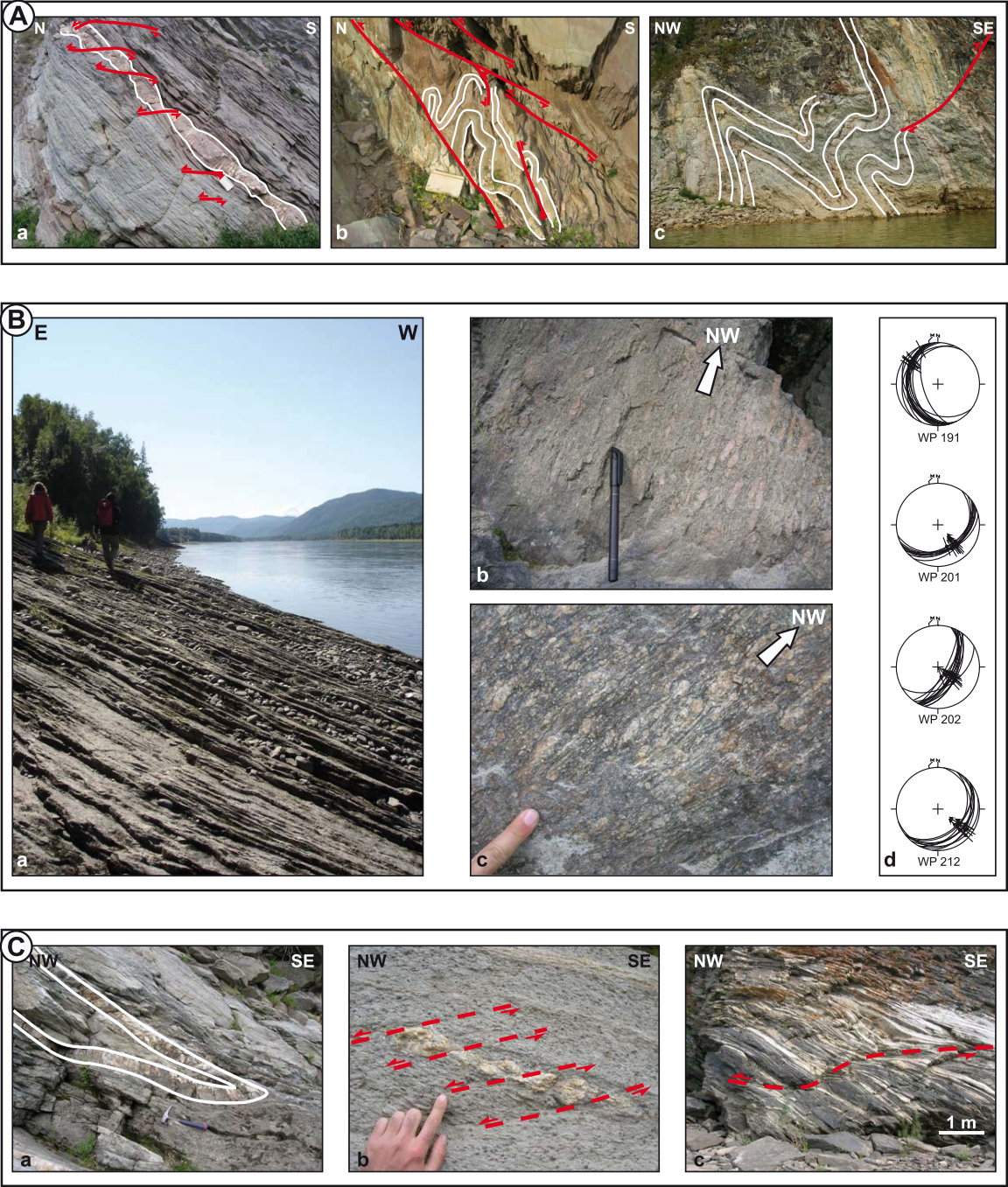
A
N
S
a
N
S
b
NW
SE
c
B
E
W
a
NW
b
NW
c
WP 191
WP 201
WP 202
WP 212
d
C
NW
SE
a
NW
SE
b
NW
SE
1 m
c

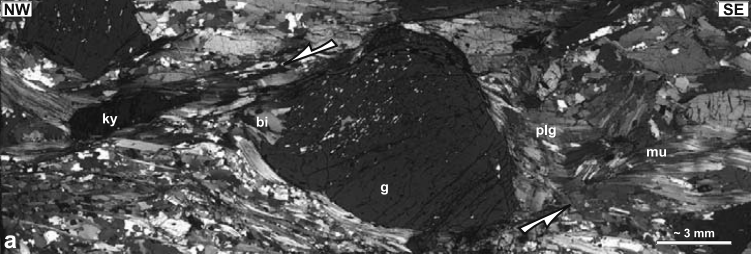

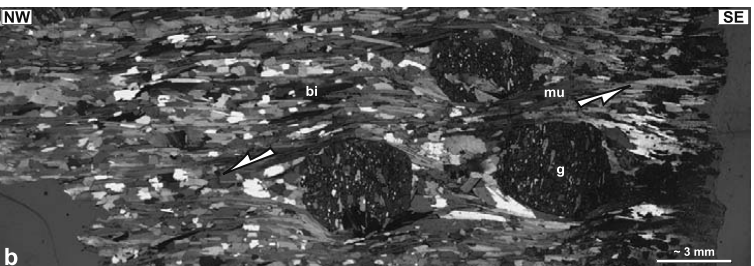

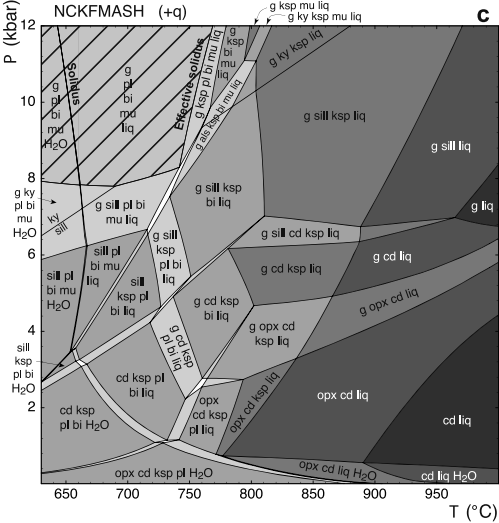

After *White et al., 2001*

g : garnet, pl : plagioclase feldspar, ksp : K feldspar, bi : biotite, mu : muscovite, ky : kyanite, sill : sillimanite, opx : orthopyroxene, cd : cordierite, liq : liquid

Estimated domain for the observed peak metamorphism conditions (sample PA0660, thin section a)

Foreland domain ← → Inner range

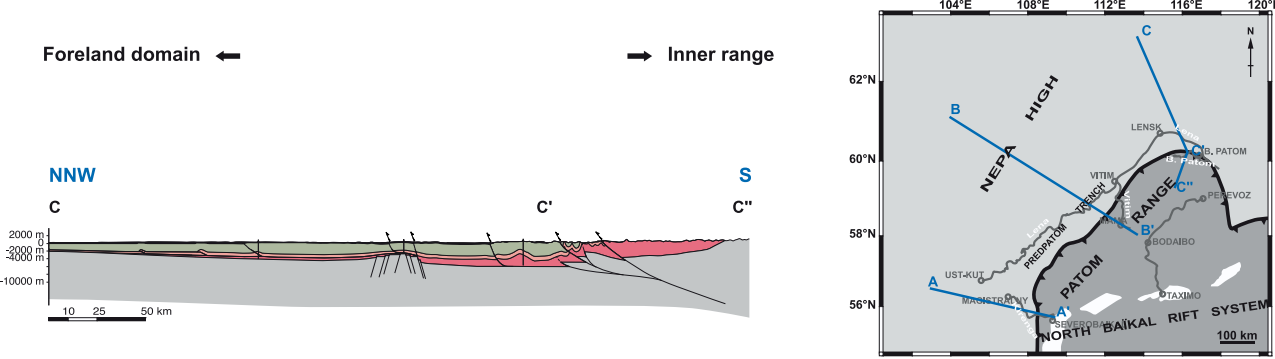

JURASSIC
SILURIAN / DEVONIAN
ORDOVICIAN
CAMBRIAN
VENDIAN
RIPHEAN
Basement
Deformed basement

vertical exageration x2
refer to the topographic map
for location

10 25 50 km

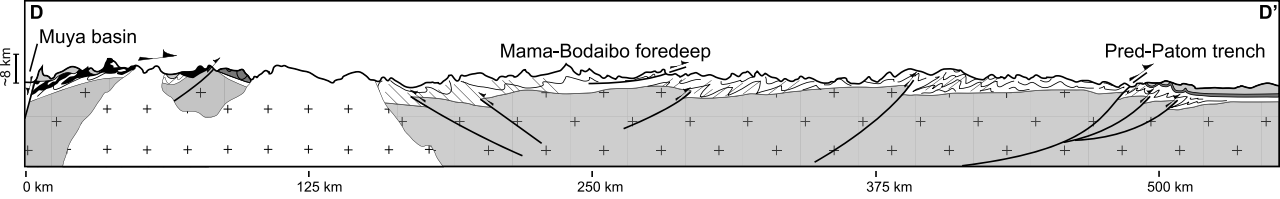
D
D
Muya basin
Mama-Bodaibo foredeep
Pred-Patom trench
~8 km
0 km
125 km
250 km
375 km
500 km

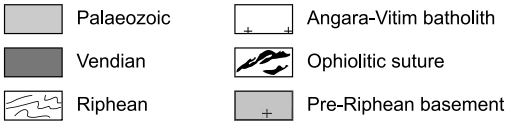
Palaeozoic
Vendian
Riphean
Angara-Vitim batholith
Ophiolitic suture
Pre-Riphean basement

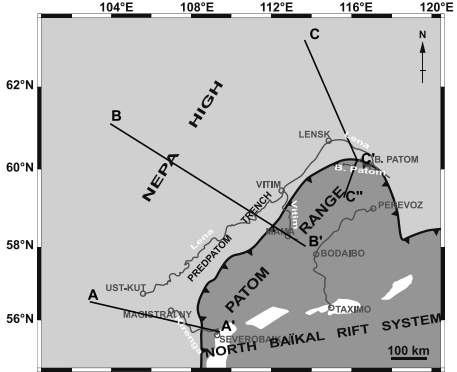
104°E
108°E
112°E
116°E
120°E
62°N
60°N
58°N
56°N
N
C
B
HIGH
NEPA
LENSK
B. PATOM
VITIM
PEREVOZ
RANGE
B'
BODAIBO
PREDPATOM
UST-KUT
A
MAGISTRALNY
PATOM
TAXIMO
A'
SEVEROBAYKALSK
NORTH BAIKAL RIFT SYSTEM
100 km

* in Ma, scale not proportional;
[1] decollements in pink are correlated, others are supposed;
[2] after Haq et al.;
[3] correlated after Khomentovsky et al., 1985, Kkomentovsky and Postnikov, 2001, Sintsov, 2005, Goddéris, 2003